PAPER • OPEN ACCESS

Thermomechanical behavior of shape memory alloy metal matrix composite actuator manufactured by composite extrusion

To cite this article: C Dahnke *et al* 2019 *Smart Mater. Struct.* **28** 055022

Recent citations

- Interface Formation and Characterization of Brass/Aluminum Compounds Fabricated Through Die Casting and Semi-Continuous Casting
Thomas Greß *et al*

- Influence of SMA-induced stress on shape memory alloy metal matrix composites manufactured by continuous composite extrusion
C Dahnke *et al*

View the article online for updates and enhancements.

Thermomechanical behavior of shape memory alloy metal matrix composite actuator manufactured by composite extrusion

C Dahnke[1] , A Reeb[2], F Pottmeyer[2], K A Weidenmann[2] and A E Tekkaya[1]

[1] Institute of Forming Technology and Lightweight Components (IUL), TU Dortmund University, Germany
[2] Institute of Applied Materials (IAM-WK), Karlsruhe Institute of Technology (KIT), Germany

E-mail: christoph.dahnke@iul.tu-dortmund.de

CrossMark

Abstract
Continuous composite extrusion represents a new possibility for the manufacturing of shape memory alloy metal matrix composites (SMA-MMC). During the process SMA wires are embedded into aluminum or magnesium profiles by means of modified porthole dies. Due to the high flexibility regarding the profile geometry, the materials as well as number, thickness and position of the SMA elements, the process can be used for the generation of a profile integrated bending function. The bending function of the actuator profile depends on the temperature and is thermally activated. The parameters influencing the behavior of the manufactured composited actuators are experimentally investigated. It is found that the radius of curvature mainly depends on the recovery stress and the eccentric position of the SMA wire as well as on the bending stiffness of the actuator profile. The bending mechanism and the experimental results are described by the use of an analytical model as well as a finite element analysis. Based on the results the analytical model is used for the targeted design of a profile with multiple embedded NiTi wires, which is able to perform a repeatable, pure elastic deflection within a defined temperature range between room temperature and 75 °C.

Keywords: shape memory alloy metal matrix composites, actuator, composite extrusion

1. Introduction

Shape memory alloys (SMA) offer unique properties such as the shape memory effect, pseudo-elasticity and a good bio-compatibility. Due to these properties SMA are highly attractive for medical applications as well as actuators in various industrial fields. Beyond that, SMA become more and more interesting as a functional material within composites. Over the last years, various approaches for the production of shape memory alloy metal matrix composites (SMA-MMC)

have been investigated. The composites possess improved mechanical properties and even show potential for an actuator functionality [1]. In the field of MMC aluminum is mainly used as matrix material due to the good formability.

To utilize the shape memory effect (SME) in a composite, Lester *et al* [2] mention two fundamental ways. The strategy of active property tuning (APT) is based on the transformation of undeformed SMA elements from the martensitic to the austenitic state, which leads for instance to an increase of the Young's modulus. The strategy of active strain energy tuning (ASET) refers to initially elongated SMA elements, which are striving to recover their original shape, when the temperature is increased to a certain material depending value. The constrained recovery leads to the induction of compressive stresses into the matrix material.

With regard to the processing of SMA-MMC, the application of the mentioned strategies is challenging. Beside the required thermomechanical treatment, the manufacturing technology has to provide sufficient bonding of both materials to transfer the occurring stresses. In this regard, Ni and Ma [3] mention casting, hot pressing, friction stir processing, ultrasonic additive manufacturing and extrusion as known processes for the manufacturing of SMA-MMC.

The most common processes are casting and hot pressing. Casting of aluminum was used by Furuya *et al* [4] to infiltrate NiTi fibers and NiTi particles [5]. Rohatgi [6] used casting as well to embed NiTi wires in aluminum. Mechanical testing of the composites showed a significant increase of Young's modulus, yield stress, work-hardening rate, resistance to fracture and ductility. Even the potential of a self-healing property could be shown. Occurring cracks could be closed due to the contraction of the NiTi wires at elevated temperatures.

Powder-metallurgy and hot-pressing were used by Miranda *et al* [7] to produce SMA-MMC from AlSi-powder and NiTi fibers. Aydogmus [8] combined magnesium powder while NiTi powder and Porter *et al* [9] used AA1090 aluminum powder and NiTi powder. Due to a high bonding quality the composites showed an increased shear strength, yield and ultimate strength as well as an increase of fatigue life.

Park *et al* [10] used hot-pressing under vacuum conditions followed by a subsequent cold-rolling process to produce TiNi/AA6061 composites. It could be shown that the crack propagation can be delayed with increasing volume fraction of the TiNi fiber. Vacuum hot pressing was also used by Armstrong and Kino [11]. AA6061 sheets were pressed on NiTi wires. Based on this work, Armstrong and Lorentzen [12] produced NiTi/AA6082 composites with the similar processing technique. Beside the increase of the yield strength, ultimate strength and fracture strain, the specimens showed a measureable plastic deformation of 2.2% caused by the contraction of the prestrained NiTi fibers after heating over the austenite-finish-temperature A_f. The achieved plastic deformation shows the potential of SMA-MMC for an actuation application.

Friction stir processing, ultrasonic additive manufacturing (UAM) and extrusion are further possibilities for the manufacturing of SMA-MMC. Ni *et al* [13] used friction stir processing for the embedding of NiTi particles in an AA6061 aluminum plate. The composite specimens showed higher strength under tensile load in comparison to non-reinforced specimens. Ultrasonic additive manufacturing (UAM) was investigated by Hahnlen *et al* [14]. The process allows a solid state bonding of thin metal layers. Due to the low processing temperatures NiTi wires with a predefined pseudo-plastic strain of the reinforcements can be embedded without the activation of the SME during manufacturing [15]. Besides the improvement of the mechanical properties, the investigations show the ability of Ni-Ti/Al composites to be used as load or strain sensors. Extrusion was used by San Martín *et al* [16] for processing of a composite, based on AA2124 aluminum powder, containing NiTi particles. The composites show improved strength and lower ductility compared to the non-reinforced specimens. Additionally, the NiTi reinforcement leads to an improved damping capacity [17].

The state of the art shows that in the field of SMA-MMC various processing technologies exists. The main focus of the investigations is on the improvement of the mechanical properties of the matrix. The use of the shape memory effect for an actuator functionality of the composite components is barely known. In the future, applications for lightweight profiles with an actuator functionality are in particular conceivable in the field of aerospace and architecture. In aerospace applications the air flow can be influenced by adaptive structures [18]. In architecture, adaptive facades which interact with the environment, can be used to reduce energy consumption and CO_2 emissions of the buildings [19]. However, up to now such investigations mainly focus on polymer matrix (PM-SMAs) or polymer composite matrix (PC-SMAs) composites [20]. One reason for this is that the processing of shape memory alloy metal matrix composites is more complicated, due to lower matrix formability and higher process temperatures. Furthermore, the manufacturing technologies mentioned above only allow the integration of SMA wires with small diameters ($\ll$1 mm). The generated recovery forces are usually too low for the generation of an actuator functionality of the metal matrix.

In Dahnke *et al* [21] the authors of this paper presented a concept for the generation of an actuator function in SMA-MMC. For the manufacturing a continuous composite extrusion process is used. The process is based on direct hot extrusion using conventional billets (figure 1). The technology is suitable for reinforcing aluminum or magnesium profiles with steel wires [22] or flat ribbons [23]. The reinforcing elements are continuously fed from outside the extrusion die through lateral channels of a feeding mandrel into the welding chamber. In the welding chamber, bonding occurs in an oxygen-free environment under high pressure (50–100 MPa) and temperature (400 °C–500 °C). The process offers a high flexibility regarding the producible profile cross sections as well as shape, thickness, number and positioning of elements. Wires up to 2 mm can be continuously embedded over the profile length. Based on the high temperature and pressure, a metallurgical bond between SMA and aluminum can be achieved [21].

Subsequently to the manufacturing process, the generation of an actuator functionality requires further processing steps [21]. Based on the hot extruded aluminum composite profile, a bending actuator needs to meet two basic requirements. First, the SMA wires have to be eccentrically embedded into the profile. Second, following the strategy of active strain energy tuning (ASET), the profile has to be stretched after the extrusion process. The stretching results in a plastic deformation of the aluminium matrix and a pseudo-plastic deformation of the NiTi wire, caused by a detwinning of the martensite. As a result of the shape memory effect, the NiTi wire is going to recover its original shape, when the temperature is increased over the austenitic start temperature A_s. In the case of a bonding between both materials, the recovery is constrained by the matrix material resulting in a high recovery stress, which is induced to the matrix. Due to
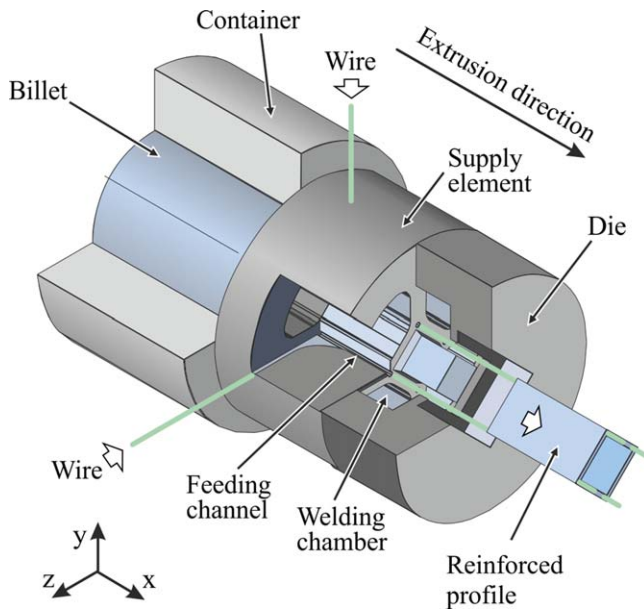
Figure 1. General principle of the composite extrusion process adapted from Pietzka and Tekkaya [24].

solid bonding between SMA and matrix as well as the eccentricity of the wire, as a result a bending moment is generated. If the bending moment is sufficiently high an elastic or even plastic deformation of the profile occurs. The experimental validation presented in Dahnke *et al* [21] shows the functionality of the concept. It could be shown that the recovery stress, generated by the shape memory effect, causes a significant plastic deformation of a specimen reinforced with a single SMA wire. It could be also shown that the usable elastic spring back after cooling keeps constant, tested over 31 thermal cycles between 20 °C and 150 °C. However, up to now it has not been investigated which parameters influence the achievable deflection of the composite actuators. As a consequence, the limits of a pure elastic curvature or deflection as well as the prediction of the actuator behavior have not been investigated.

Based on the process idea and the results shown in Dahnke *et al* [21], in this paper experimental investigations are carried out to determine the main influencing factors on the generated radius of curvature. Subsequently, an analytical model as well as FEM is used to describe the bending of the actuator and to identify the transition between a pure elastic and an elastic plastic curvature of the composite. Finally, the developed methods are used for the targeted design of a profile with multiple embedded NiTi wires, which is able to perform a repeatable, elastic deflection in a defined temperature range.

2. Experimental investigations

The experimental investigations in the following sections are used to identify the main influencing factors on the resulting curvature. The experimental procedure for the manufacturing of the composite actuators as well as the thermal activation

trials are described. Subsequently, the influence of the profile geometry and the eccentricity of the embedded SMA wire is analyzed.

2.1. Manufacturing and thermal activation

For the experimental investigations circular NiTi wires with a diameter of 1.5 mm are used. The nickel (Ni) content of the alloy (SM495) is 50.5 at% and the austenite-finish-temperature A_f is 60 °C in the supplied condition. During composite extrusion the wires are embedded to a flat rectangular profile with a width of 48 mm and a thickness of 2.9 mm (figure 2(a)). AA6060 is used as matrix material. The used die allows the embedding of a maximum number of twelve wires over the profile width. With regard to the horizontal axis of the profile, the wires can be embedded centrically or eccentrically according to the z-axis (specimen type 1 in figure 2(b)). As the material properties of SMA are highly sensitive against the thermomechanical influences during the process [25], in this work, the manufacturing parameters during extrusion are kept as constant. For the matrix, circular aluminium billets with an initial diameter of 100 mm are used. The billets are preheated to 550 °C. With an extrusion ration of $R = 54,5$ and a ram velocity of 1 mm s^{-1}, the exit velocity of the profile is 54,5 mm s^{-1}. The resulting profile exit temperature is approximately 410 °C. Due to simple air cooling without any subsequent heat treatment, the aluminium matrix of the extruded profiles corresponds to a T4 condition.

To investigate the influence of the area moment of inertia and the eccentricity of the SMA wire, five different specimen geometries (figures 3(a) and 4(a)) are taken from the extruded profiles (figure 2). Thereby, two different type of specimens can be extracted from the manufactured profile (figure 2(b)). In case of specimen type 1 the eccentricity c can be achieved by a variation of the position of the feeding channel within the extrusion die (figure 1). In specimen type 2 the eccentricity c is realized by a targeted machining from the profile. In the profile or in the manufactured specimens, the eccentricity c is measured from the centroid of the NiTi wire to the centroid of the whole composite specimen using an optical microscope. After manufacturing, all specimens are prestrained to a value of $e = 2.9\%$ in a tensile testing machine Zwick Z250. The stretching causes a detwinning of the martensite phase of the SMA wires. The subsequent thermal activation is conducted in a conventional convection furnace for 15 min. With an increment of 25 °C five temperatures between 75 °C and 175 °C are investigated. As it can be seen in figure 2(c), based on the initial state, the activation of the shape memory effect at 150 °C leads to a deformation of the specimen with a constant bending radius r. Referred to the measuring length l_{ml}, the radius r as well as the deflection d are optically measured by a high resolution camera. After cooling, only the plastic part of the deflection $d_{pl;exp}$ remains. The difference between the remaining plastic deflection $d_{pl;exp}$ and the deflection at activation temperature $d_{AT;exp}$ is purely elastic and defines the possible repeatable travel of the specimen. For the following investigations both, the curvature at activation
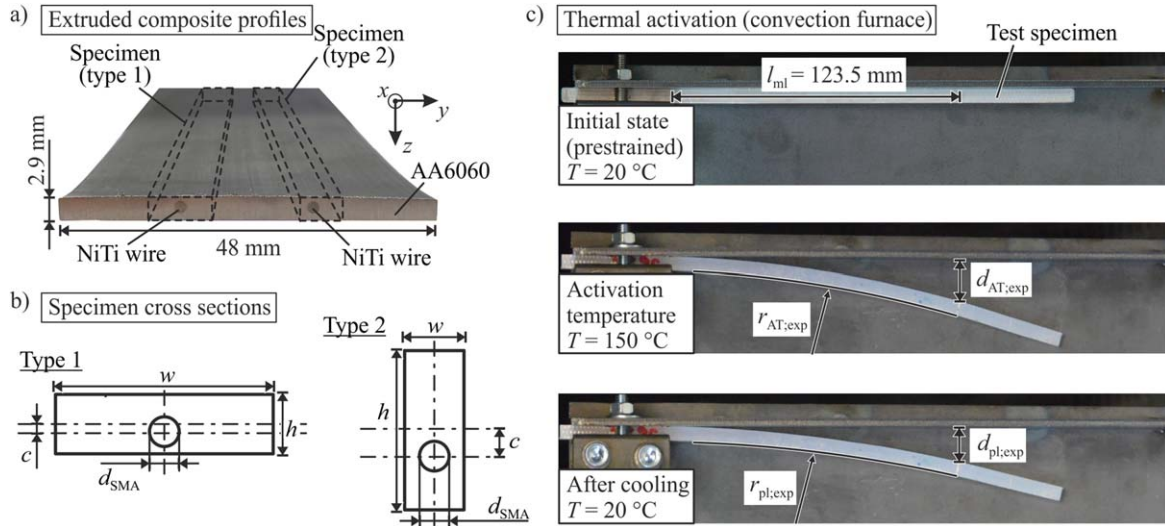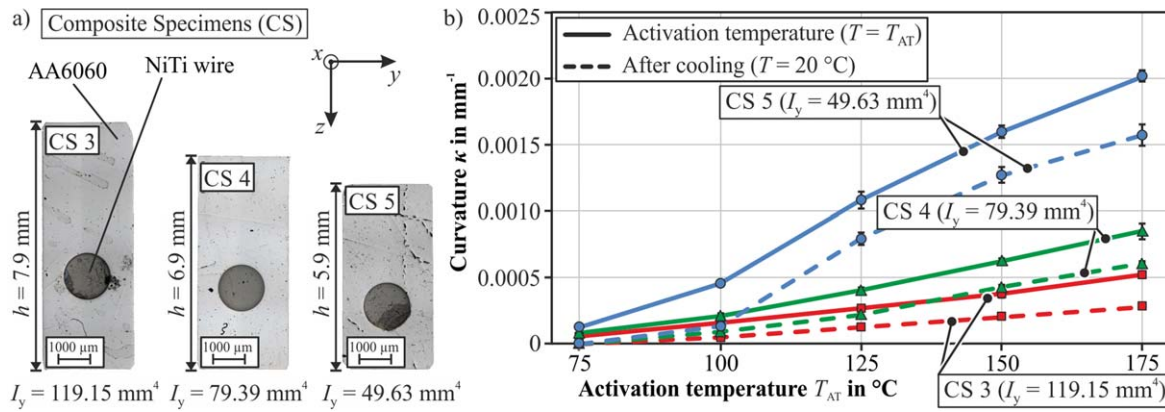
Figure 2. (a) Extruded composite profile, (b) Specimen types and preparation, (c) Thermal activation in convection furnace.
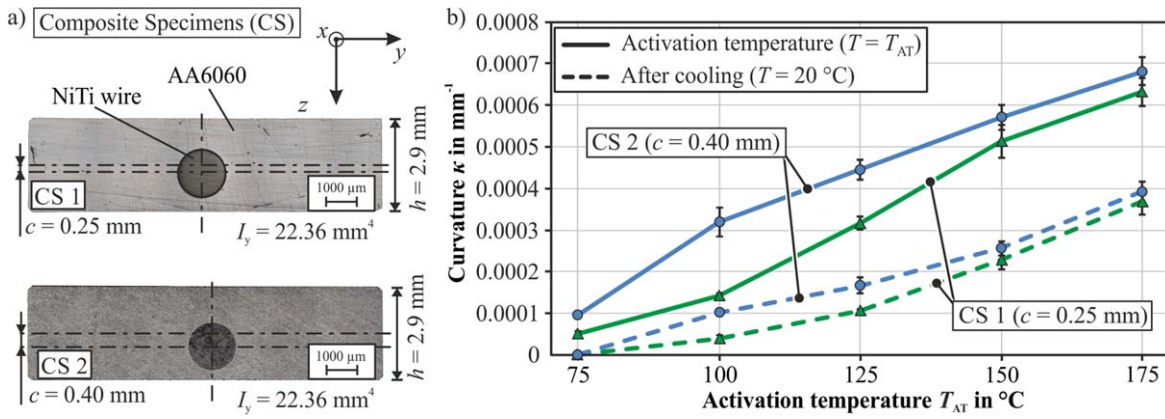
Figure 3. (a) Composite specimens with different eccentricity, (b) Influence on the resulting curvature during activation trials.

Figure 4. (a) Composite specimens with different area moment of inertia, (b) Influence on the resulting curvature during activation trials.

temperature $\kappa_{\mathrm{AT;exp}} = 1/r_{\mathrm{AT;exp}}$ as well as the remaining plastic curvature $\kappa_{\mathrm{pl;exp}} = 1/r_{\mathrm{pl;exp}}$ is evaluated.

2.2. Influence of eccentricity of the SMA wires

To determine the influence of the eccentricity of the SMA wires, according to figure 2(b), two specimens of type 1 are

investigated. The width w is 11 mm and the height h is 2.9 mm in both cases. The eccentricity referred to the z-axis in composite specimen CS 1 is 0.25 mm and in composite specimen CS 2 0.4 mm, respectively. Each trial was repeated three times. As it can be seen in figure 3(b), the curvature κ increases with increasing activation temperature as a result of the increasing recovery stress. The occurring standard

deviations are small. Referred to the eccentricity, a higher eccentricity leads to a higher curvature, due to a higher bending moment. In this case, the bending moment depends only on the lever arm, as the recovery stress of the SMA wire at similar activation temperature is the same. It can be seen that at an activation temperature of 75 °C in both specimen configurations, the curvature κ is purely elastic, as the curvature after cooling goes back to zero. Based on a straight profile and a length l_{ml} of 123.5 mm, the purely elastic deflection at 75 °C is 0.4 mm (CS 1) and 0.6 mm (CS 2).

2.3. Influence of the area moment of inertia

For the investigations of the influence of the area moment of inertia, three specimens of type 2 (figure 2(b)) are investigated. Generated by manufacturing, the eccentricity in all specimens is 1 mm according to the *z*-axis. The width *w* is 2.9 mm in all cases. To achieve different moments of inertia I_{y}, the height *h* was set to 5.9 mm, 6.9 mm and 7.9 mm. The number of repeated trials was three. In figure 4(b), the activation of the specimens shows an increase of the curvature κ with an increasing activation temperature analogue to figure 3(b). Due to the identical recovery stress as well as eccentricity, the generated bending moment at every activation temperature is the same. The resulting curvature only depends on the area moment of inertia. As expected, the curvature κ increases with a decreasing area moment of inertia I_{y}, due to a lower resistance against the deformation (figure 4(b)). Analogously to the influence of the eccentricity, it also can be seen that at an activation temperature of 75 °C in all specimen configurations there is no curvature or deflection measurable after cooling. Because there is no recovery stress left in the SMA wire, which is high enough to kept up a small part of the elastic curvature κ, it can be assumed that that nearly the full proportion of austenite has transformed to martensite during cooling.

The physical mechanisms of the bending actuator as well as the results of the experimental investigations regarding the influence of the eccentricity and the area moment of inertia are analytically described in the following sections.

3. Analytical model

The objective of the following sections is the analysis and prediction of the behavior of the actuator based on the classical beam theory. For the following analytical model an ideal bonding between SMA and matrix as well as a negligible influence of the different coefficient of thermal expansion is assumed. In the first step it is shown how the constrained recovery of the embedded wire in combination with the eccentric position results in a bending moment. Considering idealized values for the composite actuator the theoretical curvature during activation as well as the occurring stresses are described in the second step. Under consideration of the resulting stresses in the third step, the activation force of the NiTi wire is determined. Finally, the analytical model and
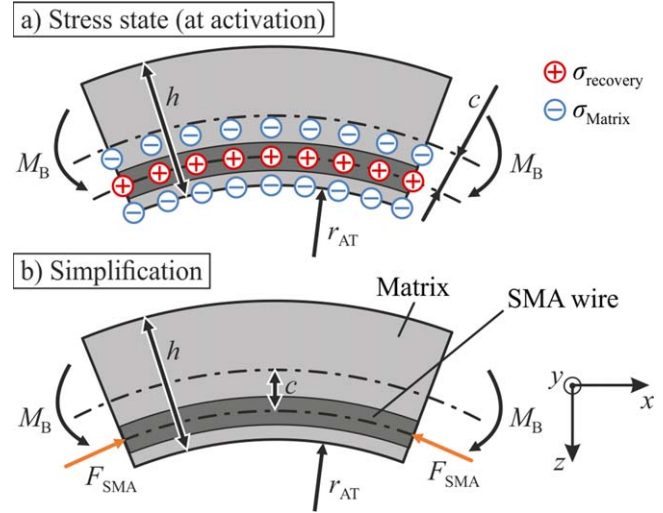

Figure 5. Longitudinal section at activation and simplification.

the experimentally determined activation force of the NiTi wire is used to predict the pure elastic deflection of the specimen geometries CS 1–CS 5 tested in section 2.

3.1. Curvature prediction

The results of the experimental investigations show a correlation between the curvature, the bending moment and the area moment of inertia. Following the classical beam theory, the curvature κ can be described as the ratio between the bending moment M_{B} and the bending stiffness EI:

$$\kappa = \frac{M_{\mathrm{B}}}{EI}. \tag{1}$$

In case of an ideal bonding between SMA and matrix during activation a tensile stress occurs within the SMA wire, due to the constrained recovery (figure 5(a)).

Based on the equilibrium of forces in the contact zone:

$$\sigma_{\mathrm{recovery}} \cdot A_{\mathrm{SMA}} = -\sigma_{\mathrm{Matrix}} \cdot A_{\mathrm{Matrix}}, \tag{2}$$

it is assumed that the recovery stress $\sigma_{\mathrm{recovery}}$ of the SMA wire can be reduced to a punctual applied compressive force F_{SMA} (figure 5(b)). Together with the eccentricity *c*, the activation force F_{SMA} determines the bending moment M_{B}.

As the composite specimens consists of two materials with different cross section and Young's modulus (figure 6(a)), the mechanical behavior is not constant over the total cross section.

For this reason, idealized values, especially the idealized centroid S_{id} (figure 6(b)), have to be determined for the curvature prediction. In the first step, the determination requires the weighting of the Young's moduli E_{SMA} and E_{Matrix}:

$$n_1 = \frac{E_{\mathrm{SMA}}}{E_{\mathrm{SMA}}} = 1 \quad \text{and} \quad n_2 = \frac{E_{\mathrm{Matrix}}}{E_{\mathrm{SMA}}}. \tag{3}$$
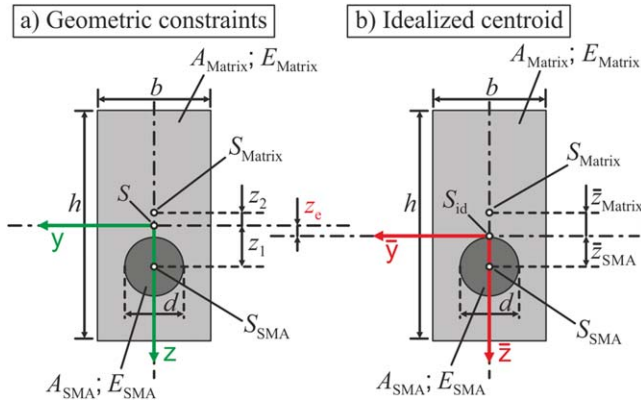
Figure 6. Geometric constraints and idealized centroid.

With equation ([3](#)) the idealized cross-sectional area $\overline{A}$ of the composite specimen can be written as:

$$\overline{A} = n_1 \cdot A_{\text{SMA}} + n_2 \cdot A_{\text{Matrix}}. \tag{4}$$

With regard to the geometric centroid of the composite specimens, the position of the idealized centroid S_{id} can then be determined by the displacement z_{e}:

$$z_{\text{e}} = \frac{1}{\overline{A}} \cdot (n_1 \cdot A_{\text{SMA}} \cdot z_1 + n_2 \cdot A_{\text{Matrix}} \cdot z_2). \tag{5}$$

The displacement z_{e} results in a shift of the centroids of the partial cross sections S_{SMA} and S_{Matrix} from the initial centroid S. With the determined distances $\overline{z}_{\text{SMA}}$ and $\overline{z}_{\text{Matrix}}$ the area moment of inertia can be calculated in both partial cross sections. These are a product of the area moment of inertia with regard to the particular centroid and the parallel axes theorem. With this, the area moment of inertia of the SMA wire I_{SMA} can be written as:

$$I_{\text{SMA}} = \frac{\pi \cdot d^4}{64} + \overline{z}_{\text{SMA}}^2 \cdot A_{\text{SMA}} \tag{6}$$

and the area moment of inertia of the matrix I_{Matrix} is:

$$I_{\text{Matrix}} = \frac{b \cdot h^3}{12} + \overline{z}_{\text{Matrix}}^2 \cdot A_{\text{Matrix}} - \frac{\pi \cdot d^4}{64} + \overline{z}_{\text{SMA}}^2 \cdot A_{\text{SMA}} \tag{7}$$

With equations ([3](#)), ([6](#)) and ([7](#)) for the idealized area moment of inertia of the composites $\overline{I}$ one can write:

$$\overline{I} = n_1 \cdot I_{\text{SMA}} + n_2 \cdot I_{\text{Matrix}}. \tag{8}$$

With equation ([8](#)), the idealized bending stiffness $\overline{EI}$ follows:

$$\overline{EI} = E_{\text{SMA}} \cdot \overline{I}. \tag{9}$$

Considering the idealized lever arm $\overline{z}_{\text{SMA}}$ determined by equation ([5](#)) as well as the correlation in equation ([9](#)), the elastic curvature κ of the specimens can be calculated to:

$$\kappa = \frac{\sigma_{\text{recovery}} \cdot A_{\text{SMA}} \cdot \overline{z}_{\text{SMA}}}{E_{\text{SMA}} \cdot \overline{I}}. \tag{10}$$
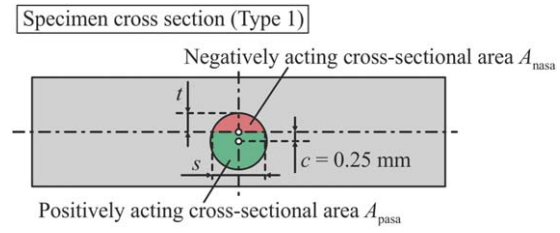

Figure 7. Positively and negatively acting cross-sectional area of the of the SMA wire.

As it can be seen in figure [7](#), in the investigated specimen type 1, one part of the SMA wire is above the horizontal axis of the composite specimen. In equation ([10](#)), the bending moment is defined by the lever arm and the recovery force of the SMA wire. As the recovery force depends on the cross section of the wire, the model would overestimate the curvature if the total cross section would be taken into account. For this reason, a simple weighting factor is used for this type of specimen. The factor is based on the ratio between the negatively acting cross-sectional area A_{nasa} and the total cross-sectional area A_{SMA} (figure [7](#)) of the wire:

$$f_{\text{w}} = 1 - \frac{A_{\text{nasa}}}{A_{\text{SMA}}}. \tag{11}$$

Considering the weighting factor f_{w}, the final description of the curvature κ can be written as:

$$\kappa = \frac{f_{\text{w}} \cdot \sigma_{\text{recovery}} \cdot A_{\text{SMA}} \cdot \overline{z}_{\text{SMA}}}{E_{\text{SMA}} \cdot \overline{I}}. \tag{12}$$

3.2. Resulting stress during thermal activation

Under consideration of the classical beam theory the axial stress σ_{x}, which occurs in the longitudinal section shown in figure [5](#), is a superposition of the normal stress generated during the thermal activation and the resulting bending stress. The normal stress in the wire corresponds to the recovery stress σ_{recovery} of the SMA acting in x-direction. The recovery stress is measured experimentally in section [3.3](#). As the recovery stress is a tensile stress, with equation ([2](#)), the compressive stress in the aluminum matrix can be calculated to:

$$\sigma_{\text{Matrix}} = -\sigma_{\text{recovery}} \cdot \frac{A_{\text{SMA}}}{A_{\text{Matrix}}}. \tag{13}$$

Considering the idealized area moment of inertia $\overline{I}$ for the idealized bending stress $\overline{\sigma}$ along the $\overline{z}$ axis (figure [6](#)) one can write:

$$\overline{\sigma} = \frac{M_{\text{B}}}{\overline{I}} \cdot \overline{z}. \tag{14}$$

From equation ([14](#)) the real bending stress in the SMA wire and the aluminum matrix can be calculated by taking into account the weighting factors of equation ([3](#)):

$$\sigma_{\text{i}} = n_{\text{i}} \cdot \overline{\sigma}. \tag{15}$$

With equations (13)–(15) the stress in the aluminum matrix $\sigma_{x,matrix}$ of the thermally activated bending actuator can be finally written as:

$$\sigma_{x,matrix} = n_2 \cdot \frac{M_B}{\bar{I}} \cdot \bar{z} - \sigma_{recovery} \cdot \frac{A_{SMA}}{A_{Matrix}}. \quad (16)$$

Analogously the stress in the SMA wire can calculated to:

$$\sigma_{x,wire} = n_1 \cdot \frac{M_B}{\bar{I}} \cdot \bar{z} + \sigma_{recovery}. \quad (17)$$

In both cases the recovery stress $\sigma_{recovery}$ has to be known.

3.3. Determination of SMA recovery stress

For the validation of the analytical model, the recovery stress of the SMA wire is determined in the following experimental investigation. As the recovery stress is influenced by the applied load as well as a certain heat treatment, in this case the process temperatures, those factors are taken into account.

Due to the strong metallurgical bond between SMA wire and matrix, the wires cannot be extracted from the profiles after the extrusion process without further influencing the material properties. As a consequence, the wires cannot be characterized after the have been exposed to the exact thermomechanical conditions. To consider the thermal load along the process chain as realistic as possible, the as delivered SMA wires are heat treated before testing in accordance to the occurring temperatures and cooling rates. For this reason, wires with a length of 200 mm are positioned in a notch between two aluminum strips with a thickness of 1.5 mm each. With a width of the strips of 48 mm and a total thickness of 3 mm, the geometric dimensions correspond to the dimensions of the extruded profile in figure 2(a). Before the SMA wires are insert, the aluminum strips are heated to 500 °C in a convection furnace. The temperature is in accordance to the temperature in the extrusion die. After the insertion of the wire, the prepared strips are kept at 500 °C for 20 s, which corresponds to the process time between which the wire enters and leaves the extrusion die. Subsequently, the prepared strips are cooled down in air, to achieve a cooling rate in accordance to the cooling rate after extrusion. All wires used in the following experimental investigations are treated as described.

Beside the influence of a certain heat treatment, it is known that the shape memory effect under zero-stress differs from the response under a certain load [26]. As the stress level influences the shape memory response, it has to be considered for the measurement of the recovery stress. Due to the hydrostatic pressure and the material flow in the welding chamber of the extrusion die, the SMA wire is exposed to a mechanical load during the manufacturing process. It cannot be excluded completely that the mechanical load has also an influence on the SMA properties. However, it assumed that a process induced strain in the SMA wire is only elastic, as the wires are embedded in the austenitic phase possessing a high strength. Furthermore, it can also be assumed that any residual stress after the extrusion process is released due to preparation of the specimens and the subsequent stretching.
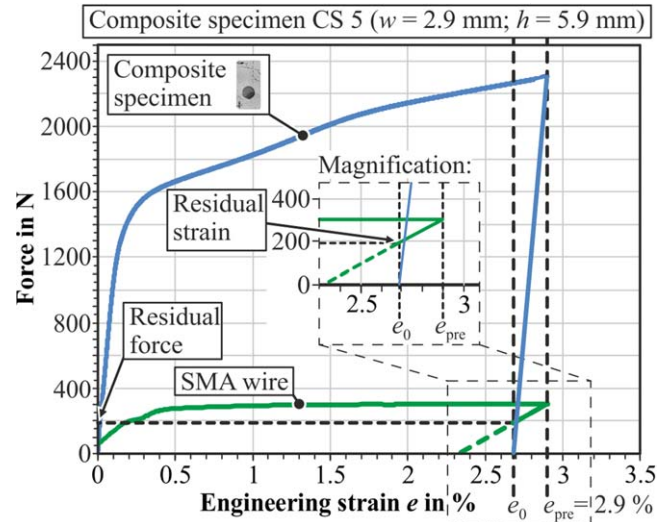
Figure 8. Residual force and strain in the SMA wire after unloading using composite specimen CS 5 with $w = 2.9$ mm and $h = 5.9$ mm as an example.

For this reason, in the following only the residual stresses after stretching are considered.

The residual stresses after stretching are caused by the difference in the Young's modulus and yield stress. They can be estimated by the evaluation of the force-displacement-diagram (figure 8). In the following, composite specimen CS 5 is used as an example. In figure 8 it can be seen that after prestraining the composite specimen to $e_{pre} = 2.9\%$, unloading leads to an elastic spring back. As a result, the plastic strain e_0 remains. If the force-strain-diagram of the SMA wire is compared with the composite, it can be seen that after the same amount of prestrain ($e_{pre} = 2.9\%$), unloading would lead to a higher elastic spring back of the wire. However, due to the solid bonding, the SMA wire can only be unloaded to e_0, determined by the composite. This leads to a residual force or stress.

For the example of CS 5 (figure 8), the residual force is approximately 190 N. As the value is positive, tensile stress results in the SMA wire. With a diameter of the wire $d = 1.5$ mm, the residual tensile stress can be calculated as approximately 107.5 MPa. Considering the equilibrium of forces in the contact zone in equation (2) as well as a constant distribution of the stress, the residual compressive stress within the matrix is approximately 12 MPa. The residual stresses in the SMA wire depend on the geometry of the composite specimens. As the differences in the geometric dimensions are only small, the determined residual stresses in all five composite specimens are between 107.5 MPa and 118 MPa. As a consequence, a mean value of 110 MPa is used for the determination of the recovery stress of the SMA wire.

Considering the mean residual tensile stress as well as the thermal load along the process chain in the next step the recovery stress is experimentally is determined by using the three stage test [27]. For the test, three heat treated wires with a length of 200 mm are used. The length in the measuring zone is 70 mm. In the first step of the three stage test
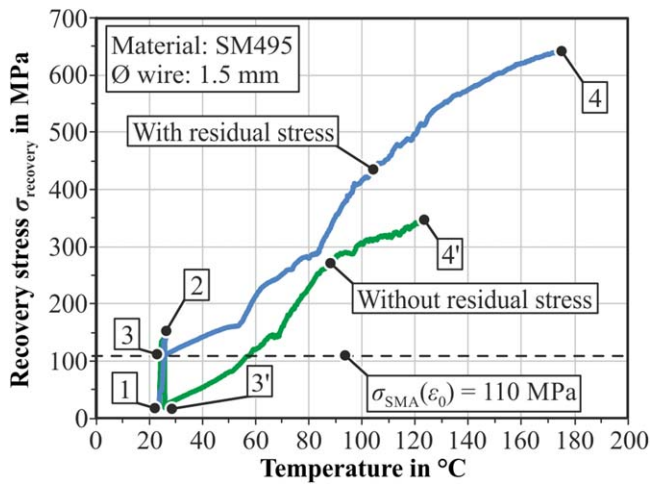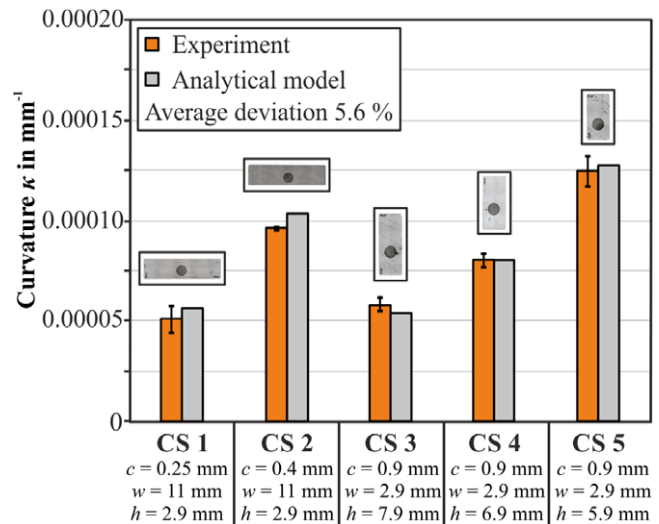
Figure 9. Measurement of the SMA recovery stress with and without consideration of the residual stresses.

Figure 10. Comparison between experimentally and analytically determined curvature κ at an activation temperature of 75 °C.

(figure 9), starting from point 1, the wire is prestrained to $e_{pre} = 2.9\%$ (point 2) at room temperature. Here, according to the martensite plateau, the necessary stress is about 150 MPa. In case of consideration of the residual stresses, the wire is unloaded to a stress level of 110 MPa (point 3) in the next step. At point 3, the displacement of the clamping jaws is fixed to provoke a constrained recovery during heating. Subsequently, the temperature is increased at up to 175 °C (point 4) resulting in the appearance of the recovery stress. For the activation temperatures investigated in this paper, the average values of the three tested wires as well as the scattering can be seen in figure 14. For a comparison, in figure 9 the measurement is also conducted without consideration of the residual stresses. In this case, the wire is completely unloaded (point 3′) after the prestraining (point 2).

3.4. Validation of analytical curvature prediction

The experimental investigations of all composite specimens (figures 3(a) and 4(a)) show a purely elastic deformation at an activation temperature of 75 °C. Under consideration of the residual stresses caused by the prior stretching, in figure 9 the average recovery stress at 75 °C is 276.4 MPa. The average value is measured from three activation trials. For the prediction of the elastic curvature using equation (12), a Young's modulus of 68 GPa is used for the aluminum at 75 °C and for the NiTi 75 GPa, respectively. The negatively acting cross-sectional area (figure 7), used for the determination of the weighting factor f_w, is assumed with $A_{nasa} \approx 2/3 \cdot s \cdot t$ based on Harris and Stöcker [28]. All other necessary parameters can be determined by equations (2) to (9).

Figure 10 shows the comparison between the experimentally and the analytically determined curvature κ. With an average deviation of 6.2% the results of the analytical prediction are in agreement with the experimental results. In case of specimen type 1 (CS 1 and CS 2) the analytical model overestimates the curvature, as in specimen type 2 (CS 3 to CS 5) underestima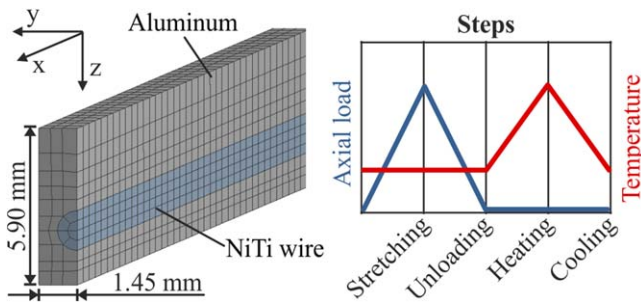tion occurs. The overestimation is caused by the negatively acting cross-sectional area above the horizontal axis of specimen type 1 (figure 7). During the thermal activation this cross-sectional area does not only reduce the applied force of the SMA wire F_{SMA} (figure 5). Actually it works against the bending, as the constrained recovery of the wire reduces the occurring tensile stress above the horizontal axis. However, the overestimation is adequately reduced by the weighting factor f_w to a maximum of 12% in case of composite specimen CS 1. This deviation is within the scatter of the experiments.

4. Numerical analysis

The results of section 3.4 show that the analytic model is able to predict the resulting curvature considering the desired elastic deformation of the bending actuators at 75 °C. Due to the simplification of the acting force of the SMA wire (figure 5) as well as the unknown behavior of the neutral fiber during the bending, the analytic prediction of the irreversible plastic curvature at higher temperatures is challenging. However, the analysis of the occurring stresses in equations (16) and (17) allow the prediction of the transition from elastic to plastic deformation. To validate these equations and to predict also the occurring elastic-plastic deformation at higher activation temperatures FEM is used. All specimen geometries (CS 1–CS 5) are simulated considering all five activation temperatures from 75 °C to 175 °C.

4.1. FE model

As the simulation of the actuators requires a coupling of thermal and mechanical load as well as a description of the shape memory effect, in this work ANSYS Workbench 16.2 is used. The implemented SMA material model, based on Souza *et al* [29] and Auricchio and Petrini [30] is suitable for three-dimensional problems. The thermomechanical behavior

Figure 11. FE model geometry for composite specimen CS 5 and modeled process steps.

Table 1. Properties of the aluminum AA6060 matrix.

Temperature	Young's modulus (in MPa)	Coefficient of thermal expansion (in $10^{-5}\,\mathrm{K}^{-1}$)	Poisson's ratio
$T = 20\,°\mathrm{C}$	69 000	2.34	0.33
$T = 75\,°\mathrm{C}$	66 930	2.34	0.33
$T = 100\,°\mathrm{C}$	64 860	2.34	0.33
$T = 125\,°\mathrm{C}$	62 790	2.45	0.33
$T = 150\,°\mathrm{C}$	60 720	2.45	0.33
$T = 175\,°\mathrm{C}$	58 650	2.45	0.33

is modeled in four process steps, stretching, unloading, heating and cooling (figure 11) in accordance with the experimental procedure in section 2. Using symmetry on the xy-plane for all five geometries a half model is used. The length of all specimens is 120 mm and corresponds to the measurement length l_{ml} of the experiments before stretching. Both the aluminum matrix and the SMA wire are meshed with 3D-twenty-node structural elements (SOLID186). With a minimum edge length of 0.29 mm in the wire and 0.42 mm in the matrix, the number of elements for composite specimen CS 5 is 2040. For the transmission of the recovery stress from the SMA wire to the matrix, bonded contact is defined in the interface using Augmented Lagrange formulation with a stiffness factor of 10.

4.2. Material parameters for the aluminum matrix

The elastic properties of the AA6060 aluminum are given in table 1 as a function of the temperature. The values are deduced from literature, as the Young's modulus of aluminum decreases between room temperature and 200 °C by about 15% [31]. The temperature depending values for the coefficient of thermal expansion are taken from the data sheet of the aluminum supplier (BIKAR-METALLE GmbH). For the plastic behavior isotropic hardening is considered. The data is experimentally determined by conventional tensile tests for every activation temperature T_{AT} up to $\varepsilon = 0.12$. As the expected plastic deformation for the actuators are low, an extrapolation of the flow curves is not necessary.

4.3. Material parameters for the SMA wire

Regarding the SMA material model, for the martensite phase ($T = 20\,°\mathrm{C} < M_{\mathrm{f}}$) the Young's modulus is 21 000 MPa and the coefficient of thermal expansion is $6.6 \cdot 10^{-6}\,\mathrm{K}^{-1}$. For the austenite phase ($T = 75\,°\mathrm{C} > A_{\mathrm{f}}$) the Young's modulus is 79 000 MPa and $1.1 \cdot 10^{-}\,\mathrm{K}^{-1}$ is the coefficient of thermal expansion. Beside Young's modulus and coefficient of thermal expansion, the model for the shape memory effect requires seven parameters (table 2), which can by experimentally identified by the stress-strain and stress-temperature diagrams of the pure SMA wire. In Dahnke *et al* [21] it was shown that the stress-strain behavior and the shape memory effect of the heat treated SMA wire is in agreement with the experimental results. The behavior of the composite actuator can be modeled

over all four process steps. However, in comparison to the experimental results, it was not possible to predict the deflection at activation temperature $d_{\mathrm{AT;exp}}$ and the remaining deflection $d_{\mathrm{pl;exp}}$ after cooling (figure 2(c)). The numerically determined values were more than 100% below the experimentally measured values. The reason for the deviation can be found in the experimentally identified parameters for the SMA material model. As SMA are highly sensitive for thermal and mechanical influences, the properties change during the manufacturing process. In composite extrusion, the occurring temperatures depend on various parameters like, extrusion velocity, initial billet temperature, extrusion ratio, die design and cooling rate of the profile. As the embedded wire cannot be extracted from the extruded profile without a further influencing of the properties, the direct identification of the exact material parameters is not possible. The short term heat treatment to 500 °C and the subsequent cool down with a cooling rate comparable to the cooling rate of the aluminum profiles does not give the correct parameters, either.

The deflection of the bending actuator strongly depends on the amount of the recovery stress during the thermal activation. Based on the SMA material model introduced by Souza *et al* [29] and Auricchio and Petrini [30], the temperature dependent scaling parameter β has a significant effect on the generated recovery stress. Due to this, in Dahnke *et al* [21] it was suggested to fit the β parameter to the experimentally measured deflection for every activation temperature. It could be shown that with the fitted β parameter an agreement between the experimental and numerical deflection could be achieved. However, as only a single actuator geometry was tested in Dahnke *et al* [21] a transferability of the identified parameters has not been shown yet. For this reason, in the following section, the methodology of the inverse parameter identification is verified by using the results of the activation trials of the five investigated specimen geometries (CS 1 to CS 5) in section 2.

4.4. Inverse parameter identification

As the FE model of geometry CS 5 (figure 11) requires the smallest number of elements, it is taken as reference for the inverse identification of the β parameter to save computational time. In the first step, a SMA parameter set for the martensite phase (20 °C) and for the austenite phase (75 °C) is experimentally determined (table 2). In the second step the
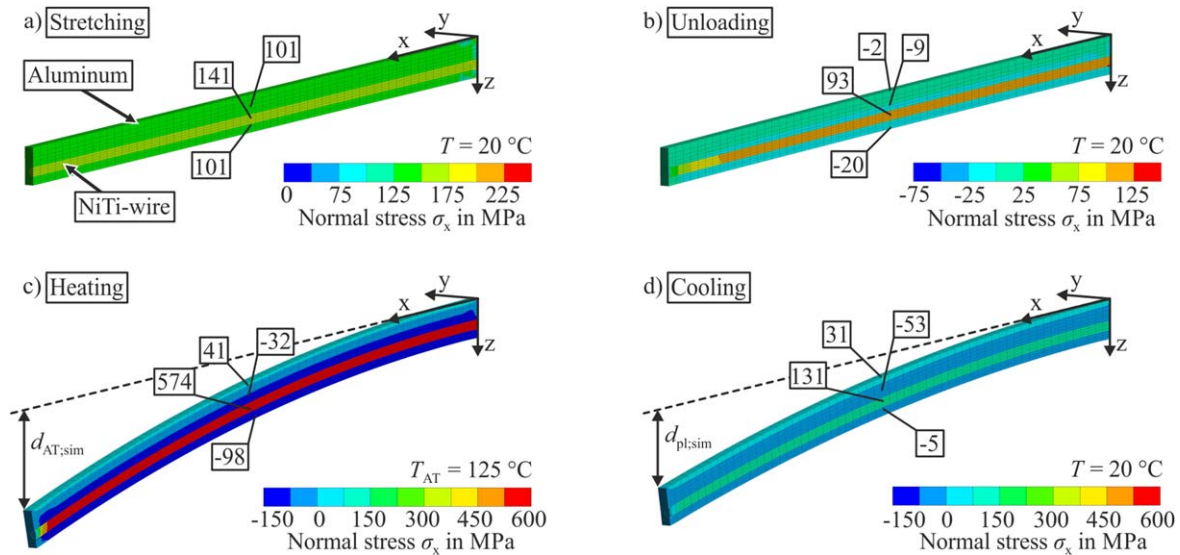
Figure 12. Behavior of the simulated actuator (CS 5) along the four process steps (activation temperature $T_{AT} = 125\ ^{\circ}$C).

Table 2. Temperature depending parameter set.

Temperature T	Hardening parameter h (in MPa)	Reference temperature T_0 (in °C)	Elastic limit R (in MPa)	Temperature scaling parameter β^{a} (in MPa °C^{-1})	Maximum transformation strain $\bar{\varepsilon}_L$	Martensite modulus E_m (in MPa)	Lode dependency parameter m
$T = 20\ ^{\circ}$C	163	45	120	2.50	0.062	37 000	0
$T_{AT} = 75\ ^{\circ}$C	1250	45	220	7.80	0.062	37 000	0
$T_{AT} = 100\ ^{\circ}$C	1250	45	220	10.52	0.062	37 000	0
$T_{AT} = 125\ ^{\circ}$C	1250	45	220	8.20	0.062	37 000	0
$T_{AT} = 150\ ^{\circ}$C	1250	45	220	6.47	0.062	37 000	0
$T_{AT} = 175\ ^{\circ}$C	1250	45	220	3.97	0.062	37 000	0

[a] fitted parameter.

stretching, unloading, heating and cooling of geometry CS 5 is simulated (figure 12). The deflection at activation temperature $d_{AT;sim}$ (figure 12(c)) and the deflection after cooling $d_{pl;sim}$ (figure 12(d)) are evaluated and compared with the experimentally obtained values (figure 2(c)).

If the numerically determined values are not in agreement with the experimental ones, in the third step the β parameter is fitted until the numerical results match to the experimental results. As the behavior of the SMA wire as well as of the aluminum is not linear, the β parameter has to be fitted for every activation temperature T_{AT}. Table 2 shows the final parameter sets for the SMA model for all five activation temperatures.

Following the described procedure, the recovery stress can be found for every activation temperature T_{AT} which is responsible for the generated deflection of the actuator. As it can be seen from figure 13, for the composite specimen CS 5 an agreement between the deflection at activation temperature d_{AT} and the deflection after cooling d_{pl} can be achieved. The average deviation over the five activation temperatures is 29.7%. It has to be noted that the level of the average deviation is mainly influenced by the deviation between $d_{pl;exp}$ and $d_{pl;sim}$ at an activation temperature of 75 °C. At this

temperature in the experiments an average deflection of 0.11 mm was measured. In the simulation, on the contrary, the deflection is 0.39 mm. This results in a deviation of 254%. For nearly all other activation temperatures the deviation is in the range of 5%. The reason for the high deviation at 75 °C is discussed in section 5.

4.5. Analysis of the occurring stresses

Figure 12 shows the occurring normal stress in x-direction over the four process steps. In accordance to the experimental procedure described in section 2, in figure 12(a) the composite specimen (CS 5) is prestrained by $e_{pre} = 2.9\%$. Due to the different mechanical properties, in the SMA wire the resulting tensile stress is 141 MPa and 101 MPa in the aluminum matrix, respectively. In the second process step (figure 12(b)) the load is relieved, which results in elastic spring back and residual stresses. Corresponding to the experimental investigations in figure 8, residual stresses occur in both components of the composite specimen due to the difference in the Young's modulus and the yield stress. As expected, tensile stress remains in the SMA wire and compressive stress remains in the matrix. Regarding the occurring tensile stress in the wire, the numerical
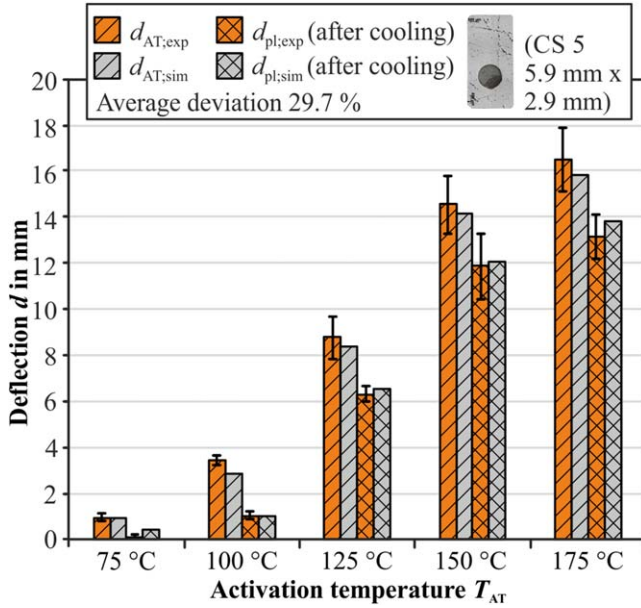
Figure 13. Comparison between experimentally and numerically determined deflection of the composite specimen CS 5 for all activation temperatures.
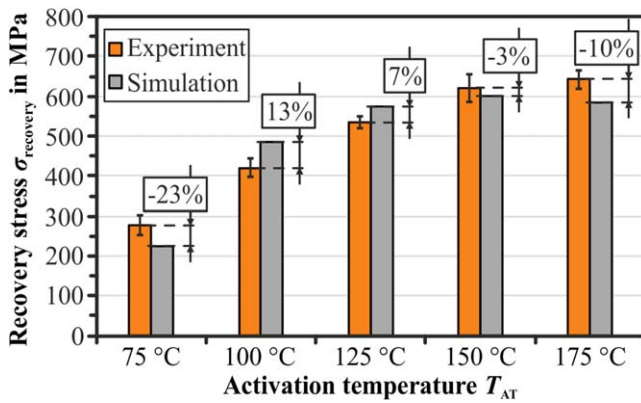
Figure 14. Comparison of the numerically and experimentally determined temperature depending recovery stress.

value of 93 MPa (figure 12(b)) shows an agreement compared to the 107.5 MPa determined from the stress-strain diagram (figure 8). In the third process step the specimen is heated. In figure 12(c) an activation temperature of $T_{AT} = 125$ °C is chosen exemplarily. It can be seen that due to the thermal activation in the SMA wire a tensile stress of 574 MPa is generated. As a consequence of the eccentric embedding in the matrix a tensile stress of 41 MPa occurs on the upper side and a compressive stress of −98 MPa occurs on the bottom side. The gradient of the stress distribution results in the deflection of the actuator $d_{AT;sim}$. Evaluating the amount of the generated recovery stress $\sigma_{recovery}$ over all five activation temperatures, it can be seen from figure 14 that the values are in agreement with the experimentally determined values.

In the last process step the actuator is cooled down back to room temperature (figure 12(d)). As the generated stress in

the matrix during the heating exceeded the flow stress of the aluminum, after cooling the plastic deflection $d_{pl;sim}$ remains. Only the elastic deflection springs back and residual stresses remain in the actuator.

To predict the undesired beginning of the plastic deformation in dependence of the recovery stress of the SMA wire, it has to be estimated when the generated stress in the matrix overcomes the flow stress of the aluminum. In both components the generated stress during the bending can be calculated by equations (16) and (17) if the recovery stress $\sigma_{recovery}$ is known. The experimental investigations in section 2 have shown that the transition between a pure elastic and an elastic plastic deformation of all actuators lies between 75 °C and 100 °C. For this reason, in figure 15 the stresses are evaluated along a path in the middle of the simulated composite specimen CS 5 at 75 °C (figure 15(a)) and at 100 °C (figure 15(b)). Considering all six components of the stress tensor it can be seen that during the thermal activation only a significant stress in x-direction occurs. All other components can be neglected as they are nearly zero. As the stress distribution is homogenous over the considered cross section and no shear stresses occur, the thermal activation of the actuators can be characterized as pure uniaxial bending. If the numerically determined stress in x-direction σ_x is compared to the analytically calculated stress using equations (16) and (17) an agreement can be observed. With regard to the analytic stress distribution it must be distinguished between the usage of the recovery stress determined from the experiments and from the simulation (figure 14). By using the value from the simulation qualitatively as well as quantitatively an agreement can be seen. If the experimentally determined value is used, a quantitative deviation can be observed which corresponds to the deviation in the recovery stress as shown in figure 14. Looking at the temperature depending yield stress of the prestrained aluminum matrix ($\varepsilon = 0.027$) it can be seen from figure 15(a) that the yield stress of the matrix σ_y is not exceeded at any point. In comparison, at an activation temperature of $T_{AT} = 100$ °C (figure 15(b)), the analytically determined stress reaches the yield stress of the aluminum matrix at the bottom side of the actuator. The results show that equations (16) and (17) can be used to estimate the maximum recovery stress $\sigma_{recovery}$ in dependence of the temperature which must not be exceeded to prevent an undesired plastic deformation. This means that for the design of a simple composite actuators a numerical analysis is not essential.

4.6. Transferability of the SMA material parameters

To identify the parameters for the SMA material model the actuator specimen CS 5 (figure 4(a)) is used as a reference geometry. As the manufacturing conditions in the experiments (extrusion velocity, extrusion ratio, profile exit temperature, cooling rate) are the same for all specimen geometries, it is expected that for every temperature the same recovery stress is generated during the thermal activation. This means that the resulting deflection should be predictable in the other four specimen geometries. For this reason, in the following the specimen geometries CS 1 to CS 4 are simulated with the identified parameters (table 2). An activation
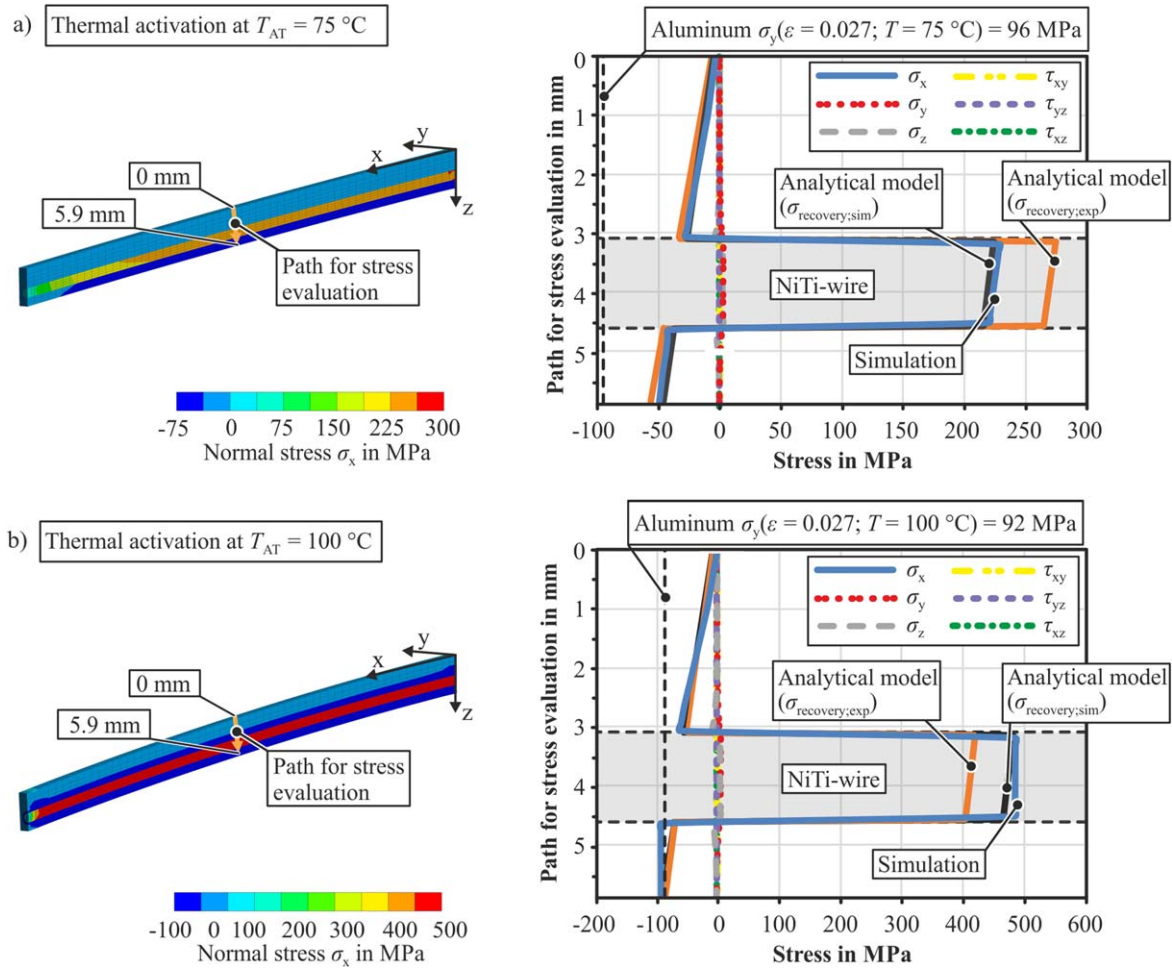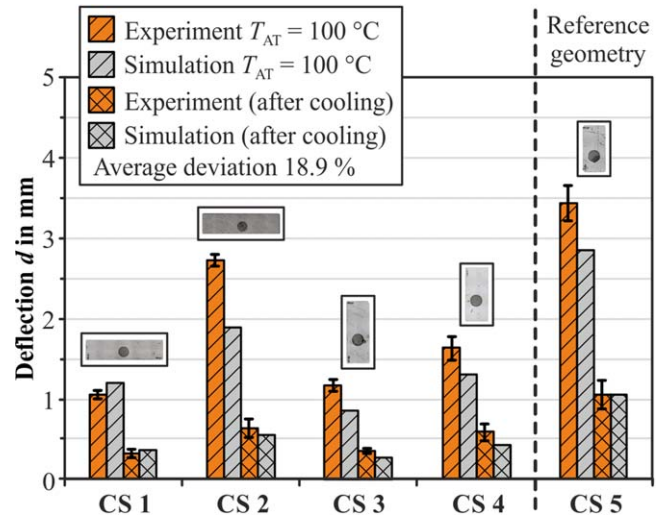
Figure 15. Comparison of the numerically and experimentally determined axial stresses σ_x at (a) 75 $^\circ$C and (b) 100 $^\circ$C.

temperature of $T_{AT} = 100$ $^\circ$C is chosen exemplarily. Figure 16 shows the comparison between the experimentally measured and the numerically determined values. With an average deviation of 18.9% the obtained results are in agreement. Reasons for the deviations can be found in measuring inaccuracies or variations of the temperature during the manufacturing. Especially the variation of the temperature can have a considerable influence as the SMA wires are highly sensitive regarding the temperature. Controlling the temperature of the die or the exit temperature of the profile is still challenging during extrusion.

However, considering the small deviations which have been obtained, the transferability of the identified parameters to the other specimen geometries validates the methodology. In dependence of the activation temperature, the parameters can be used to model even more complex profile geometries as long as they are manufactured with the same process parameters.

Figure 16. Comparison between experimentally and numerically determined deflection of all five specimens at $T_{AT} = 100$ $^\circ$C.

5. Design of an actuator profile

With regard to the overall objective, in this section a profile with a repeatedly usable actuator function is manufactured.

The profile should have the ability to perform a purely elastic bending, when the temperature is increased. If a straight profile is required at room temperature for structural reasons, after cooling no plastic deformation should remain. However, depending on the desired application, it is also conceivable

that the actuator profile is designed to perform an elastic travel between two pre-established curvatures. In this case, initially an elastic-plastic curvature is generated due to heating to a higher temperature in the first heating cycle. Subsequently, the curvature can be changed purely elastic between the initial maximum temperature and a temperature below the maximum temperature.

To demonstrate the eligibility of the developed analytical and numerical methods for the profile design, the flat rectangular profile from figure 2(a) is used. The profile has a width of 48 mm and a height of 2.9 mm. Based on the experiments the temperature range for the actuator operation should be between 20 °C and 75 °C. To use the identified parameters (table 2) at the activation temperature $T_{AT} = 75$ °C for the design of the profile, the process parameters for the manufacturing must be the same. As heat treatment and prestrain significantly influence the SMA response, those values must be kept as constant as well. If the exit temperature of the profile for example increases due to an increasing ram velocity, the inverse identification of the β parameter (experiment and simulation) has to be performed again. For this reason, the final profile has to be manufactured with a ram velocity of 1 mm s^{-1} and simple air cooling after extrusion. The prestrain must be $e_{pre} = 2.9\%$ corresponding to the prestrain used before.

With the mentioned requirements, it is possible to determine the necessary number of SMA wires by the ratio of the area moment of inertia between the demonstrator profile $I_{y;Dem}$ and the composite specimen CS 2 (figure 3(a)). The ratio can be calculated to:

$$n = \frac{I_{y;Dem}}{I_{y;CS\,2}} = 4, 36. \quad (18)$$

The single reinforced specimen CS 2 has an eccentricity of $c = 0.40$ mm and shows a pure elastic curvature at an activation temperature of $T_{AT} = 75$ °C. No curvature remains after cooling back to room temperature (figure 3(b)). Assuming a linear correlation between the number of SMA wires n and the recovery stress $\sigma_{recovery}$, the demonstrator should achieve the same curvature as specimen CS 2 with a number of $n = 4.36$ wires. Therefore, the eccentricity has to be $c = 0.40$ mm and the activation temperature $T_{AT} = 75$ °C as well. For the analytical prediction of the curvature, in equation (12) the coefficient for the number of wires n has to be added. With this, the resulting curvature κ can be written as:

$$\kappa = \frac{f_w \cdot \sigma_{recovery} \cdot n \cdot A_{SMA} \cdot \bar{z}_{SMA}}{E_{SMA} \cdot \bar{I}}. \quad (19)$$

As the experiments have been carried out with SMA wires with a diameter of 1.5 mm and only full wires can be embedded, the number of required wires is set to a number of $n = 4$. As it can be seen in figure 17 the wires are positioned symmetrically in the profile to achieve a homogenous curvature.

After manufacturing, the composite profile is prestrained to the required value of $e_{pre} = 2.9\%$. The measurement length l_{ml} is 430 mm. Subsequently, the demonstrator is activated in
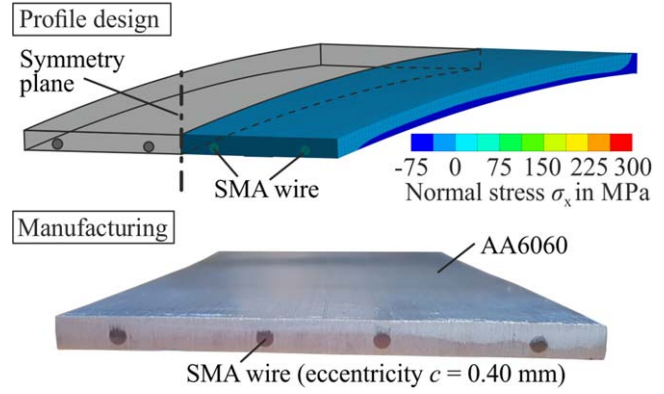

Figure 17. Design and cross section of the manufactured demonstrator profile.

the convection furnace at $T_{AT} = 75$ °C. As it can be seen in figure 18(b), the activation of the SME results in a radius of curvature of $r_{AT;exp} = 11\,725$ mm. The resulting deflection at $l_{ml} = 430$ mm is measured to 7.88 mm. During cooling, the deflection goes back to zero. The experiment shows that the actuator profile can perform a repeatedly travel between 20 °C and 75 °C. It can be seen in table 3 that the experimental results are in agreement with the analytical results as well as with the simulation. As the actuator generates a constant curvature, the achieved deflection depends on the considered measurement length. At a measurement length of $l_{ml} = 1000$ mm, for instance, a theoretic deflection of 42.6 mm can be achieved.

Analogously to the evaluation of composite specimen CS 5 in figure 13, after heating to 75 °C in the simulation a remaining deflection can be determined when the actuator is cooled back to room temperature (table 3). As shown in figure 18(c), in the experiment the deflection goes completely back to zero after the first heating cycle. However, before the first heating cycle directly after stretching a deflection of 1.39 mm can be seen (figure 18(a)).

Based on the equilibrium of forces in equation (2), after stretching the tensile stress in the SMA wire leads to a compressive stress in the aluminum matrix. With regard to the simulated composite specimen CS 5 in figure 12(b) the influence of residual stresses after stretching can be seen. As the wire is eccentrically embedded in the matrix, a gradient of the stress distribution from −2 MPa to −20 MPa occurs. Due to the stress gradient a slight bending moment is already generated after stretching. In the simulated specimen CS 5, this bending moment leads to an elastic deflection of 0.39 mm which corresponds to the remaining deflection at an activation temperature of 75 °C in figure 13. As the deformation at 75 °C is only elastic, in the simulation the remaining deflection after cooling is equal to the deflection after stretching. The residual stresses remain in the components.

In comparison, in the experiments it can be seen that due to the residual compressive stress after stretching an elastic deflection remains as well (figure 18(a)). However, in contrast to the simulation the deflection is zero after cooling in the experiment (figure 18(c)). The residual stress is relieved due
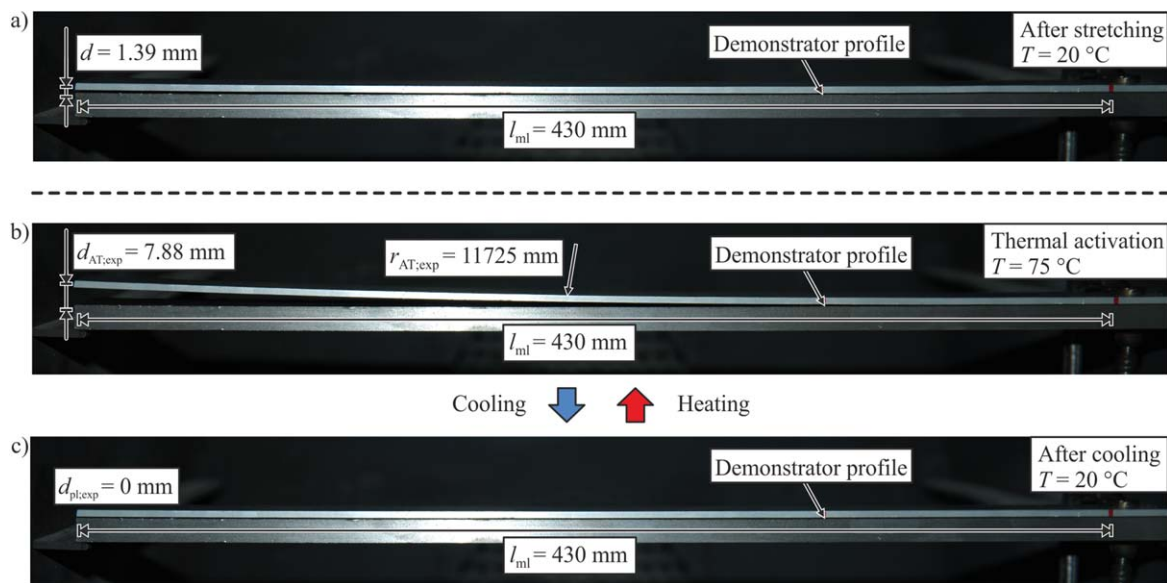
Figure 18. Thermal activation of the manufactured demonstrator profile at $T_{AT} = 75$ °C.

Table 3. Determined deflection of demonstrator profile.

Deflection d	Experiment (in mm)	Analytical model (in mm)	Simulation (in mm)
$T = 20$ °C	0	0	2.85
$T = 75$ °C	7.88	8.06	9.56

to the thermal activation of the profile which cannot be represented in the simulation.

6. Conclusions

Continuous composite extrusion allows the manufacturing of SMA-MMC with a thermally activated actuator functionality. The following conclusions can be made:

- The resulting curvature of the composite actuators is mainly influenced by the area moment of inertia, the eccentricity of the embedded SMA wire as well as the amount of applied temperature depending recovery stress.
- The analytical model is able to predict the pure elastic curvature as well as the stress distribution. Due to the knowledge of the stress distribution, the beginning of an undesired plastic deformation can be estimated.
- The stress distribution of the actuator can be analyzed by means of FEM. As only one significant normal stress is present the thermal activation can be characterized as pure uniaxial bending caused by an inner force.
- A correct prediction of the resulting actuator deflection requires a reverse identification of the material parameters of the SMA material model, as the properties are changing during the manufacturing process and the embed wires cannot be extracted from the profile after extrusion.

- The analytical and numerical methods are transferable to any profile or specimen, as long as they are manufactured with the same process parameters (extrusion velocity, extrusion ratio, profile exit temperature, cooling rate, etc).
- A change in the process parameters (extrusion velocity, extrusion ratio, profile exit temperature, cooling rate, etc) requires a new identification of the acting recovery stress. However, the developed methodologies are transferable to any related bending actuator geometry.

ORCID iDs

C Dahnke ⓘ https://orcid.org/0000-0002-4078-9603

References

[1] Miracle D B 2005 Metal matrix composites—from science to technological significance *Compos. Sci. Technol.* **65** 2526–40
[2] Lester B, Baxevanis T, Chemisky Y and Lagoudas D 2015 Review and perspectives: shape memory alloy composite systems *Acta Mech.* **226** 3907–60

[3] Ni D R and Ma Z Y 2014 Shape memory alloy-reinforced metal-matrix composites: a review *Acta Metall. Sin.* **27** 739–61

[4] Furuya Y, Sasaki A and Taya M 1993 Enhanced mechanical properties of Ni-Ti shape memory Fiber/Al matrix composite *Mater. Trans. JIM* **34** 224–7

[5] Furuya Y 1996 Design and material evaluation of shape memory composites *J. Intell. Mater. Syst. Struct.* **7** 321–30

[6] Rohatgi P K 2014 Al-shape memory alloy self-healing metal matrix composite *Materials Science & Engineering* A **619** 73–6

[7] Miranda G, Carvalho O, Silva F S and Soares D 2013 Effect of sintering stage in NiTi short-fibre-reinforced aluminium–silicon composites interface properties *J. Compos. Mater.* **47** 1625–31

[8] Aydogmus T 2015 Processing of interpenetrating Mg–TiNi composites by spark plasma sintering *Materials Science and Engineering:* A **624** 261–70

[9] Porter G A, Liaw P K, Tiegs T N and Wu K H 2001 Fatigue and fracture behavior of nickel-titanium shape-memory alloy reinforced aluminum composites *Materials Science and Engineering,* A **314** 186–93

[10] Park Y C, Kang J H, Lee J K, Lee G C and Furuya Y 2007 Effect of cold rolling on fatigue crack propagation of TiNi/Al6061 shape memory composite *Smart Mater. Struct.* **16** 982–8

[11] Armstrong W D and Kino H 1995 Martensitic transformations in a NiTi fiber reinforced 6061 aluminum matrix composite *J. Intell. Mater. Syst. Struct.* **6** 809–16

[12] Armstrong W D and Lorentzen T 2002 Large self-thermal-plastic deformation in a NiTi shape-memory alloy fiber-actuated aluminum metal-matrix composite *Metallurgical and Materials Transactions* **33** 3595–3540

[13] Ni D R, Wang J J, Zhou Z N and Ma Z Y 2014 Fabrication and mechanical properties of bulk NiTip/Al composites prepared by friction stir processing *J. Alloys Compd.* **586** 368–74

[14] Hahnlen R, Dapino M J, Short M and Graff K 2009 Aluminum-matrix composites with embedded Ni-Ti wires by ultrasonic consolidation *SPIE Proc.: Industrial and Commercial Applications of Smart Structures Technologies* vol 729010.1117/12.817036

[15] Hahnlen. R 2012 Characterization and modeling of active metal-matrix composites with embedded shape memory alloys *Dissertation.* The Ohio State University

[16] San Martín D, Risanti D D, Garcés G, Rivera Diaz del Castillo P E J and van der Zwaag S 2009 On the production and properties of novel particulate NiTip/AA2124 metal matrix composites *Materials Science and Engineering* A **526** 250–2

[17] Thorat R R, Risanti D D, San Martín D, Garces G, Rivera Díaz del Castillo P E J and van der Zwaag S 2009 On the transformation behaviour of NiTi particulate reinforced AA2124 composites *J. Alloys Compd.* **477** 307–15

[18] Schick J R, Hartl D J and Lagoudas D C 2012 Incorporation of shape memory alloy actuators into morphing aerostructures *Morphing Aerospace Vehicles and Structures.* ed J Valasek (UK: John Wiley & Sons, Ltd, Chichester) (https://doi.org/10.1002/9781119964032.ch10)

[19] Loonen R C G M, Trčka M, Cóstola D and Hensen J L M 2013 Climate adaptive building shells: state-of-the-art and future challenges *Renewable and Sustainable Energy Reviews* **25** 483–93

[20] Schrooten J, Michaud V, Parthenios J, Psarras G C, Galiotis C, Gotthardt R, Manson J-A and van Humbeeck J 2002 Progress on composites with embedded shape memory alloy wires *Materials Transactions* **43** 961–73

[21] Dahnke C, Shapovalov A and Tekkaya A E 2017 Thermally activated lightweight actuator based on hot extruded shape memory metal matrix composites (SMA-MMC) *Procedia Engineering* **207** 1511–6

[22] Klaus A, Schomäcker M and Kleiner M 2004 First advances in the manufacture of composite extrusions for lightweight constructions *Light Metal Age* **62** 12–21

[23] Dahnke C, Pietzka D, Haase M and Tekkaya A E 2014 Extending the flexibility in the composite extrusion process *Procedia CIRP* **18** 33–8

[24] Pietzka D and Tekkaya A E 2001 Herstellung von Verbundprofilen durch strangpressen, VDI Fortschritt-Berichte *Integration von Umformen, Trennen und Fügen für die flexible Fertigung von leichten Tragwerkstrukturen* **2** 27–47

[25] Pinter P, Reeb A and Weidenmann K A 2015 The influence of stress and heat on the transformation behavior of NiTi for actuator applications in extruded aluminum matrix composites *Mater. Sci. Forum* **825–826** 205–12

[26] Hartl D J and Lagoudas D C 2008 Thermomechanical characterization of shape memory alloy materials *Shape Memory Alloys.* ed P K Kumar and D C Lagoudas (New York: Springer Science+Business Media) pp 53–120

[27] Šittner P, Vokoun D, Dayananda G N and Stalmans R 2000 Recovery stress generation in shape memory Ti$_{50}$Ni$_{45}$Cu$_5$ thin wires *Materials Science and Engineering,* A **286** 298–311

[28] Harris J W and Stöcker H 1998 *Handbook of Mathematics and Computational Science.* (Berlin: Springer)

[29] Souza A, Mamiya E and Zouain N 1998 Three-dimensional model for solids under-going stress-induced phase transformations *European Journal of Mechanics—A/Solids* **17** 789–806

[30] Auricchio F and Petrini L 2004 A three-demensional model describing stress-temperature induced solid phase transformations: solution algorithm and boundary value problems *Int. J. Numer. Methods Eng.* **61** 807–36

[31] DIN EN 1999-1-2 2010 *Eurocode 9: Bemessung und Konstruktion von Aluminium-tragwerken—Teil 1-2: Tragwerksbemessung für den Brandfall.* (Berlin: Beuth Verlag GmbH)